Research Article

Daniel J. Apo and Shashank Priya*

High Power Density Levitation-Induced Vibration Energy Harvester

Abstract: We report a levitation-induced vibration energy harvester based on a double-repulsion configuration in the moving magnet composite. Computational modeling clearly illustrated the advantages of the double-repulsion configuration over the single-repulsion and no-repulsion configurations. Double-repulsion configuration provided the best dynamics (displacement and velocity) and output response (voltage). Based on the modeling results, an AA battery-sized harvester with the double-repulsion configuration was fabricated. The harvester exhibited high power response at low frequencies (12.9 mW at 1g and 16 Hz) and also exhibited a high normalized power density at low excitations (15.33 mW $cm^{-3}g^{-2}$ at 0.25g and 13 Hz). The harvester was used to charge a cellphone at 4.7 V DC.

Keywords: electromagnetic energy harvesting, vibration energy harvesting, nonlinear approach, system design and modeling, magnetic levitation, high power

***Corresponding author: Shashank Priya,** Center for Energy Harvesting Materials and Systems (CEHMS), Bio-Inspired Materials and Devices Laboratory (BMDL), Virginia Tech, Blacksburg, VA 24061, USA, E-mail: spriya@vt.edu
Daniel J. Apo, Center for Energy Harvesting Materials and Systems (CEHMS), Bio-Inspired Materials and Devices Laboratory (BMDL), Virginia Tech, Blacksburg, VA 24061, USA,
E-mail: djapo55@gmail.com

Introduction

Vibration-based energy harvesting devices are typically designed to scavenge mechanical energy from sources such as heavy machinery, railways, trucks, bridges, and ships. These natural sources typically vibrate at low excitations, below 0.5g (where $1g = 9.8\ m/s^2$), and low frequencies, below 20 Hz (Singh et al. 2012). Piezoelectric cantilever-based devices have recently become popular for harvesting energy from vibrations (Aktakka, Peterson, and Najafi 2011; Qi et al. 2012; Zhou, Apo, and Priya 2013). However, these devices present a fundamental challenge when designed for small-scale applications, since the resonance frequency of the structure increases as the dimension decreases (Apo, Sanghadasa, and Priya 2013, 2014). Thus, most currently reported cantilevers operate at frequencies higher than 50 Hz (Marin, Bressers, and Priya 2011). Furthermore, cantilever-based devices are generally devoid of broadband behavior at their resonance frequencies, therefore limiting their capability outside the resonance region (Mann and Sims 2009).

A promising solution for low frequency–low excitation energy harvesting is the development of magnetic levitation systems. These systems exhibit nonlinear stiffness profile due to the repulsive force between magnetic poles that varies as the square of the distance between them. The nonlinear stiffness profile in turn results in nonlinear frequency response which allows harvesting more power in a broader range of frequencies when compared with the linear frequency response observed for most of the piezoelectric devices. Several studies have identified broadband response and high power response from different forms of nonlinear magnet-based energy harvesters. A small subset of these studies (Dallago, Marchesi, and Venchi 2010; Mann and Sims 2009; Saha et al. 2008) have reported a more direct method of harvesting energy by magnetic levitation of a magnet (or magnet composite) between two stationary magnets placed in a repelling direction to the magnet composite. Tornincasa et al. (2012) analyzed this configuration for energy scavenging in automotive tires. Marin et al. have conducted considerable work in this field with the development of a pen harvester (Marin et al. 2012) and a broadband system (Marin et al. 2013).

The literature on magnetically-levitated energy harvesters has not addressed the design of efficient magnet and coil configurations which would maximize the power output at low frequencies. In this study, we present a levitation-induced vibration energy (LIVE) harvester that incorporates a double-repulsion magnet composite levitated between two stationary magnets. The coil configuration was designed to target the regions of high

magnetic flux density around the moving magnet composite. Finite element modeling and mathematical modeling were used to analyze the force field, magnetic flux, dynamics, and output response of the harvester. The models were also used to identify the advantages of the double-repulsion configuration over other possible configurations. Lastly, an AA battery-sized harvester was designed, fabricated, and tested based on the modeling results. The harvester was found to exhibit significantly high power density across different frequencies and base excitations. The harvester was also used to charge a cellphone via an external circuit.

Design, fabrication, and testing

The harvester configurations modeled in this study are shown in Figure 1. The design of the harvester fabricated and characterized is shown in Figure 1c and d. As shown in this figure, a magnetic ring composite was levitated by placing it in a repelling configuration between two stationary disk magnets in a tube with 14 mm outer diameter (od), 10.5 mm inner diameter (id), and 40 mm height. The properties of the harvester components are listed in Table 1. The magnets were designed from NdFeB N42 type material and were obtained commercially (K&J Magnetics, USA). It was important to ensure that the stationary magnet diameter was greater than the inner diameter of the moving magnet composite to prevent magnetic attraction at high displacement amplitudes where the moving magnet composite comes in close vicinity to the stationary magnets.

As shown in Figure 1c, the fabricated moving magnet composite was composed of a unique double-repulsion configuration in which three magnets (each with dimensions 9.5 mm od × 3.2 mm id × 4.8 mm height) were assembled with repelling poles and separated with carbon steel rings (dimensions 9.5 mm od × 3.2 mm

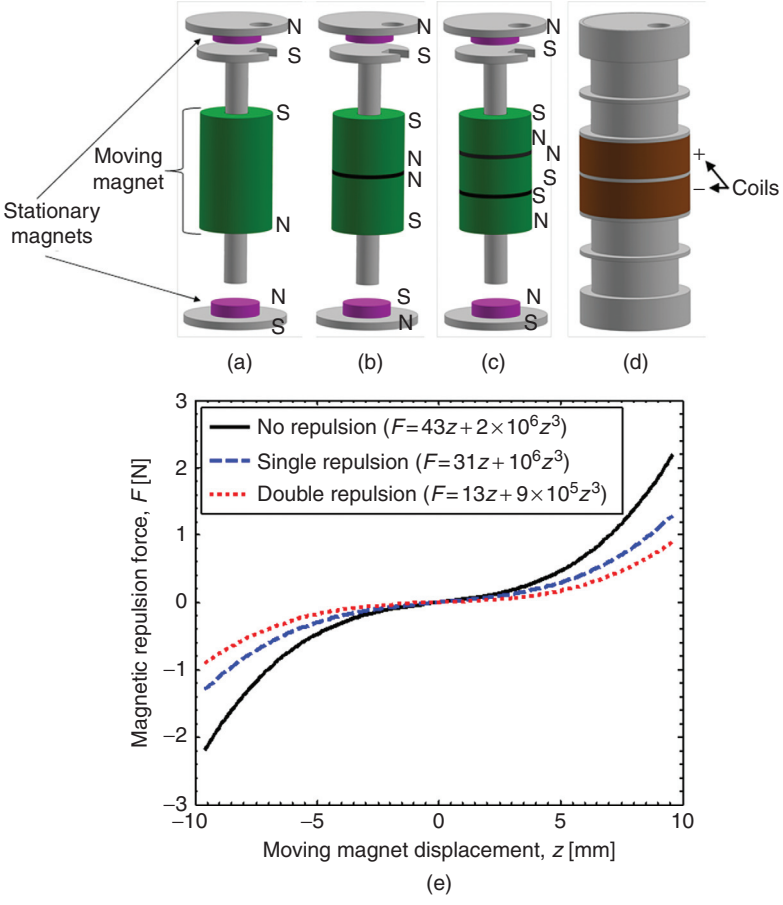

Figure 1 Design configurations of the harvester: (a) single moving magnet (no-repulsion) configuration, (b) two moving magnets (single-repulsion) configuration, (c) the fabricated three moving magnets (double-repulsion) configuration, (d) coil and casing design for the fabricated double-repulsion configuration, and (e) predicted magnetic repulsion force vs moving magnet displacement relationship for all three configurations

Table 1 Properties of the LIVE harvester components (all configurations)

Component	Properties
Harvester casing dimensions (mm)	14 od × 10.5 id × 40 long
Magnet material	NdFeB N42
Moving magnet composite dimensions (mm)	9.5 od × 3.2 id × 15.3 thick
Moving magnet composite mass (grams)	7.29
Carbon steel ring dimensions (mm)	9.5 od × 3.2 id × 0.5 thick
Carbon steel ring mass (grams)	0.25
Stationary magnet dimensions (mm)	6.4 od × 0.8 thick
Stationary magnet mass (grams)	0.2
Coil material	Copper
Each coil segment (mm)	14 od × 11 id × 4.8 thick
Coil resistance	14.43 Ω/m
Coil diameter (mm)	44 μm
No. of coil turns per segment	2,800

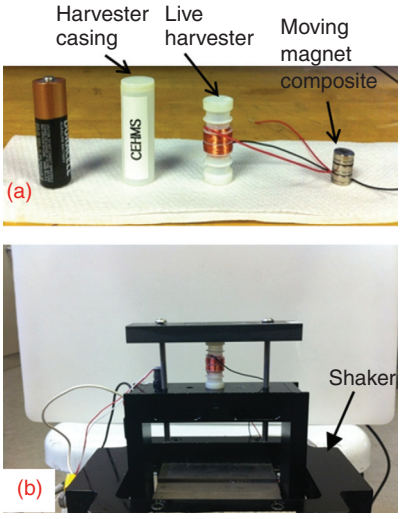

Figure 2 The fabricated LIVE harvester with double-repulsion configuration: (a) beside an AA battery and (b) in a vibration testing setup

id × 0.5 mm height). The reason for the double-repulsion design was to create two strong regions of high magnetic flux density (*B*-field). Two coil segments, each with dimensions of 14 mm od × 11 mm id × 4.8 mm height, were wound around the tube in opposite directions and aligned with the regions of high *B*-field around the moving magnet composite. This magnet and coil configuration ensures effective use of the coils and the absence of the constant zero voltage regions (magnet outside the coil area, or cancellation effects) during operation since the coils have the same height as one of the magnets in the levitating composite and the coils were wound in opposite directions. Also, the spacing between the coils equals the height of one carbon steel ring in the moving magnet composite. The center pole which guides the moving magnet composite is essential for limiting the friction. Reduction in friction can be obtained by ensuring the moving magnet composite is always concentrically located within the device thus longitudinally aligning its axis with those of the coils and stationary magnets.

The moving magnet composite was assembled using Loctite epoxy (Henkel Corp., USA) and clamped together for two days to allow the epoxy set properly. The copper coils were wound in two segments with each segment being wound in a direction different from the other and each having 2,800 turns of coil. The total coil resistance was measured to be 2,800 Ω implying an average of 0.5 Ω per turn. The coil wire had a resistance of 14.43 Ω/m and a diameter of 44 μm. The moving magnet composite was assembled by bonding the stationary magnets to the tube caps using epoxy. The LIVE harvester was tested with a standard energy harvesting setup as shown in Figure 2. A SigLab box was connected to a computer and was used as an input for an accelerometer (attached to the shaker), a laser vibrometer (pointed at the moving magnet composite), and a resistance box (to supply load resistance). The SigLab also provided the voltage response recordings from the harvester.

Modeling

A finite element model (ANSYS v14) was used to obtain the force field (solid 236 elements) and magnetic flux (solid 96 elements), while a mathematical model was used to simulate the dynamics and voltage response of the harvester. The dynamics of the oscillating moving magnet composites in the three different configurations were mathematically modeled by using a nonlinear spring-mass-damper mechanical system with an externally applied base excitation given as:

$$m\ddot{z}(t) + c_m\dot{z}(t) + c_e(t)\dot{z}(t) + kz(t) + k_3z(t)^3 = -m\ddot{y}(t) - mg \quad [1]$$

where m is the moving magnet composite mass, c_m is the mechanical damping constant, $c_e(t)$ is the instantaneous electrical damping, k is the linear stiffness constant of the spring, k_3 is the nonlinear stiffness constant of the spring, $\ddot{z}(t)$ is the relative acceleration between the base of the structure $\ddot{y}(t)$ and the vibrating mass $\ddot{x}(t)$, g is the gravitational constant, $\dot{z}$ and z are the velocity and displacement of the moving magnet composite respectively. The

acceleration of the vibrating mass $\ddot{x}(t)$ includes the moving magnet and the base of the structure also, i.e. $z(t) = x(t) - y(t)$. Thus, the value of z defines the vibration of the moving magnet only. Gravitational force is normally included in the analysis of vibrating nonlinear systems (unlike linear systems) to account for the nonlinear stiffness constant (Zavodney and Nayfeh 1989). The nonlinear mathematical spring refers to the repulsion between the moving magnet composite and the stationary magnets, and it is related to the instantaneous magnetic repulsion force (F) and the moving magnet displacement by:

$$F(t) = kz(t) + k_3 z(t)^3 \quad [2]$$

This relationship is shown for all three moving magnet configurations in Figure 1e. It can be seen that the double-repulsion configuration is the least stiff of all the three configurations and that the stiffness of the system (value of k) decreases as the number of magnets in the moving magnet composite increases (with the overall moving magnet height remaining the same). The stiffness terms were estimated by fitting the computational data with a third-order nonlinear polynomial curve as described by eq. [2]. Furthermore, it is clear from the stiffness relations that the configuration of the moving magnet composite contributes significantly to the stiffness of the entire system. This can be seen from the static magnetic force relation between two repelling cylindrical magnets which is estimated as:

$$F(d) = \frac{\mu_0 M^2 A^2 (h+r)^2}{4\pi h^2}\left[\frac{1}{d^2} + \frac{1}{(d+2h)^2} + \frac{2}{(d+h)^2}\right] \quad [3]$$

where $F(d)$ is the static repulsion force between the magnets, μ_0 is the permeability of the medium between the magnets, M is the magnetization of the magnets, A is the surface area common to both magnets, r is the radius of the magnet with the smaller diameter, h is the average height of the two magnets (or magnet composites) involved, and d is the distance between the magnets. Therefore, the repulsion force of the moving magnet composite toward the stationary magnets is smallest in the double-repulsion configuration since the limiting factor as shown in eq. [3] is the magnetization (M) between the two magnets involved (and magnetization varies with size). For example, the magnetization of the top stationary magnet in the double-repulsion configuration is caused mainly by the top magnet in the moving magnet composite.

In order to solve the dynamic system, the damping terms, c_m and c_e, were obtained and added to the model. The mechanical damping constant is defined by:

$$c_m = 2\zeta_m\sqrt{km} \quad [4]$$

where ζ_m is mechanical damping ratio. The damping ratio can be empirically determined by measuring the amplitude of displacement decay after the moving magnet composite was initially displaced from its rest position. This approach assumes a linear decay and therefore allows the damping ratio to be obtained from:

$$\ln\left|\frac{A_0}{A_n}\right| = \frac{2\pi n\zeta_m}{\sqrt{(1-\zeta_m{}^2)}} \quad [5]$$

where A_0 is the first amplitude of motion, and n is the decaying cycle. The damping ratio was calculated as 0.047. The electrical damping was estimated from:

$$c_e(t) = \frac{(B(t)\times l)^2}{R_e + R_l} \quad [6]$$

where $B(t)$ is the instantaneous magnetic flux density, l is the length of coil, R_e is the total coil resistance, and R_l is the optimum coil resistance. The B-field values apply to the instantaneous B-field region cutting through the coil. The values of coil length and resistance for the model were based on the configuration in Figure 1d using a coil factor of 0.54. The coil factor is the volume fraction of the coil compartment that is actually occupied by the coil. The total load resistance obtained was 2,900 Ω, and the optimum coil resistance applied was 4,000 Ω.

The mathematical model was also used to predict the output response of the harvester by discretizing the coil volume and applying looping forms of the equations below:

$$V = \frac{Bl\dot{z}}{R_L + R_e}R_L, \quad V_{\text{rms}} = \sqrt{\frac{1}{n}\sum_{i=1}^{n} V_i^2} \quad [7]$$

$$P = \left(\frac{Bl\dot{z}}{R_L + R_e}\right)^2 R_L \; P_{\text{rms}} = \sqrt{\frac{1}{n}\sum_{i=1}^{n} P_i^2} \quad [8]$$

where n is the number of discrete points applied.

Results

Modeling results

The predicted displacement amplitudes across different frequencies at 0.25g base excitation are shown in Figure 3. As shown, the effects of gravity and stiffness were evident in the rest position (mean displacement) of the moving magnet composites. The rest position

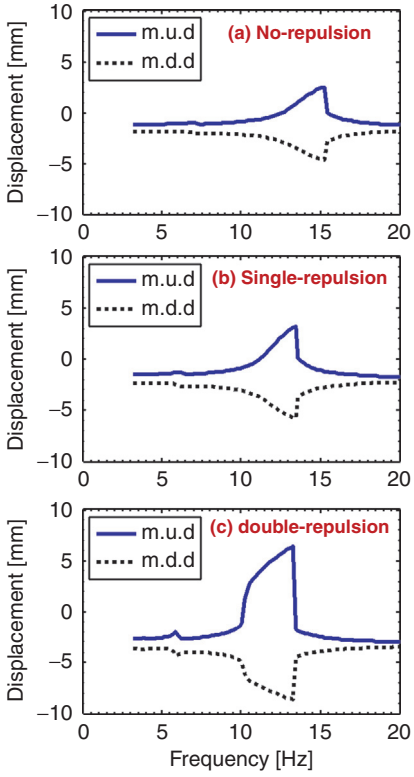

Figure 3 Predicted displacement of the three moving magnet composites at base excitation of 0.25*g*. m.u.d = maximum upward displacement and m.d.d = maximum downward displacement. (a) no-repulsion within the moving magnet composite, (b) single-repulsion within the moving magnet composite, and (c) double-repulsion within the moving magnet composite

increased downward as the moving magnet composite was modified from no-repulsion to double-repulsion. However, the maximum amplitude of displacement at resonance was less in the downward direction when compared with the upward direction across all configurations. This was more pronounced in the double-repulsion configuration, and it was due to the difference in the instantaneous repulsion force between the moving magnet composite and the stationary magnets as described in eq. [3] (because of the rest position of the moving magnet composite). Overall, the double-repulsion configuration exhibited the highest displacement amplitude at resonance.

The predicted resonance frequencies across all configurations showed a decreasing pattern from no-repulsion to double-repulsion as shown from their velocity profiles (at 0.25*g* base excitation) in Figure 4a. The decrease was more pronounced between the no-repulsion and single-repulsion configurations. The average values of radial magnetic flux (*B*-field) around the moving magnet composites are shown in Figure 4c. The sampled cross-sectional area was between 14 mm od and 11 mm id to specifically target the "shedding" region of the magnetic flux, and the radial *B*-field was analyzed across 24 mm height. The location of the coil was limited by the fact that the moving magnet composite required radial spacing to vibrate vertically without significant friction from the tube. As seen from the figure, the no-repulsion configuration has the weakest *B*-field profile. The single-repulsion configuration has one strong *B*-field region, but the most efficient (or optimized) height of the coil compartment for the single-repulsion configuration cannot be as easily determined as in the double-repulsion case. This is because the height of each coil segment in the double-repulsion case must equal the height of one magnet in the moving magnet composite to avoid voltage cancellation effects. The double-repulsion configuration has two strong *B*-field regions which can be targeted by two coil segments placed close to each other (and wound in opposite directions) thus creating an efficient coil/magnet configuration. Small-sized LIVE harvesters require small magnet thicknesses and can be difficult to fabricate, thus imposing a limitation on the number of magnets in the moving magnet composite. It is possible to increase the number of magnets in the moving magnet composite (for large harvesters), but such increase would cause a decrease in the magnetic flux density and shift the regions of strong magnetic field (due to repulsion) toward the moving composite and away from the coils, thus severely decreasing the energy harvesting potential of the device.

As seen in the magnetic flux profile, the summation of the magnetic flux values (when the moving magnet is at its rest position) produced a net value only in the single-repulsion case. As a result, the electrical damping term (as outlined in eq. [6]) impacted the single-repulsion configuration significantly more than the no-repulsion and double-repulsion configurations. Moving magnet composites with an even number of magnets will be affected by a higher electrical damping than those with an odd number of magnets. However, the electrical damping effect reduces as the number of magnets in the moving magnet composite increases (for even number composites). The negative impact of the electrical damping is shown in the velocity profile (Figure 4a). The resonance frequency of the single-repulsion configuration was significantly reduced, but the velocity was also negatively impacted by the electrical damping. The velocity was thus highest in the double-repulsion configuration therefore suggesting a higher voltage response for the same amount of coil around the magnets.

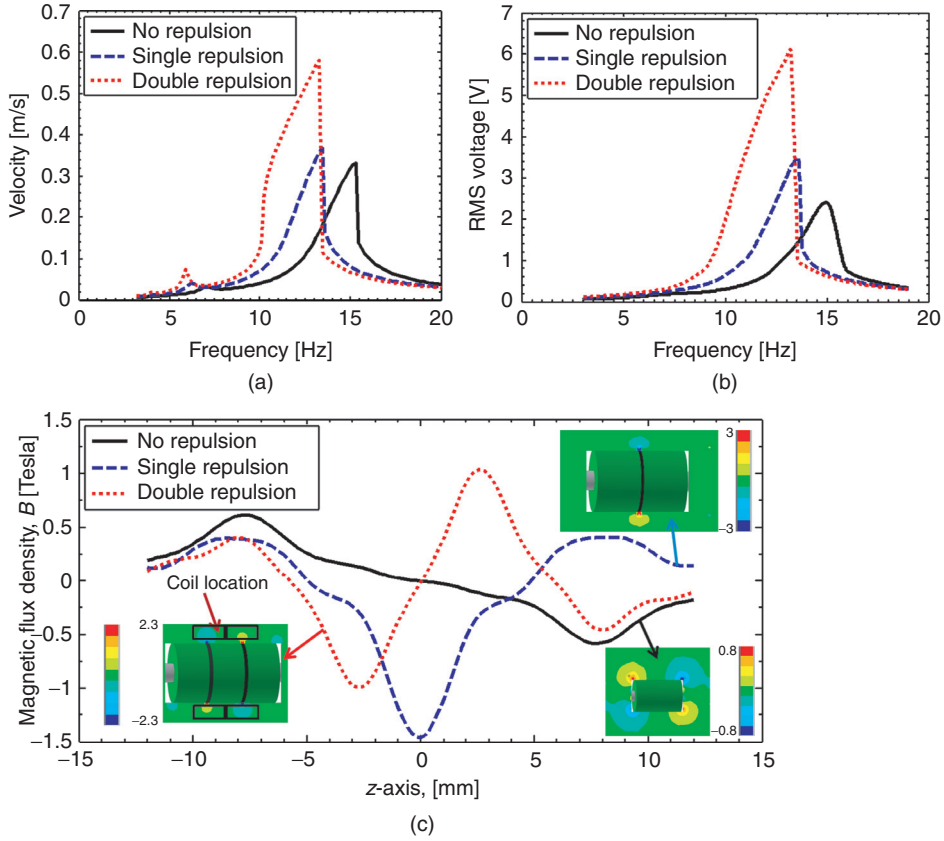

Figure 4 (a) Predicted velocity profiles across all three moving magnet configurations at base excitation of 0.25*g*, (b) predicted RMS voltage response across all three moving magnet configurations at base excitation of 0.25*g*, and (c) predicted average radial magnetic flux density around the moving magnet composites. Sampled cross-sectional area was between 14 mm od and 11 mm id

Table 2 Important factors for optimum LIVE harvester performance

Criteria	Important factor
Improved dynamics (low frequency, increased displacement amplitude, and increased velocity)	1. Increase repulsion configuration 2. Decrease moving-to-stationary magnet size ratio
Improved output response (voltage and power)	1. Centralize coil location with moving magnet rest position 2. Target regions of high *B*-field with coils 3. Reduce friction on the outer and inner regions of the moving magnet 4. Use a center pole (in the tube) to longitudinally align the axis of the moving magnet to the stationary magnets

The velocity was crucial in estimating the voltage (V) and power (P) response as expressed in eqs [7] and [8]. The voltage increases with velocity while the power response varies with the square of the velocity. Again, the *B*-field values used to obtain the voltage and power response applies to the instantaneous *B*-field region cutting through the coil. The predicted values of the root-mean-square (RMS) voltage showed similar trends when compared with the velocity profile, therefore validating the effect of the electrical damping term, and the linear relationship between velocity and the *B*-field.

From the modeling results, some important factors for optimum LIVE harvester performance (for a given tube size) were observed as listed in Table 2. Low frequency, increased displacement, and velocity can all be attained by increasing the repulsion configuration (to double-repulsion) in the moving magnet composite. Also, decreasing the ratio of moving magnet size to stationary magnet size would positively impact the dynamics of the harvester. For the voltage and power response, the coil should be placed strategically to target the regions of high *B*-field and also adjusted for the rest position of

the moving magnet composite. Limiting the friction on the outer and inner regions of the moving magnet composite positively impacts the electrical response. Furthermore, the use of a center pole in the tube to longitudinally align the axis of the moving magnet with the stationary magnets ensures that the radial magnetic flux lines are properly aligned with the coils.

Experimental results

A load optimization test was conducted by applying a varying load resistance to the coil and monitoring the RMS voltage and power response as shown in Figure 5a and b. The optimum load resistance was approximately 3,800 Ω, and it was applied via a resistor for the output response experiments. From the plots of the closed circuit RMS voltage and power variations shown in Figure 5c and d, the harvester exhibited a broadband response across a wide range of base accelerations. The resonance frequencies were approximately 13 Hz at 0.25*g*, 14.03 Hz at 0.5*g*, 15.05 Hz at 0.75*g*, and 16 Hz at 1*g*. Thus, the increase in base acceleration caused a slight increase in the resonance frequency. Also, the RMS voltage output values were approximately 4.7 V at 0.25*g*, 6.1 V at 0.5*g*, 6.75 V at 0.75*g*, and 7 V at 1*g*. The voltage response was therefore significantly greater than the 1.5 V produced at peak non-depleted performance by a standard AA battery. In comparison with the modeling results shown in Figure 4b, the experimental voltage response at 0.25*g* was consistently within 7% error. The only exception was at resonance where the sharp voltage peak in the model was not captured experimentally. The experimental RMS power response behaved in the same way as the voltage response. The harvester produced an RMS power output of 5.9 mW at 0.25*g*, 9.7 mW at 0.5*g*, 12 mW at 0.75*g*, and 12.9 mW at 1*g*.

The LIVE harvester was also compared with current state of the art electromagnetic harvesters as shown in Table 3. For low-frequency energy harvesting, the harvester exhibits comparatively high power output with increasing base excitation (12.9 mW at 1*g* and 16 Hz). However, the normalized power density is significantly higher than similar electromagnetic harvesters, especially at low base excitation (15.33 mW $cm^{-3}g^{-2}$ at 0.25*g* and 13 Hz).

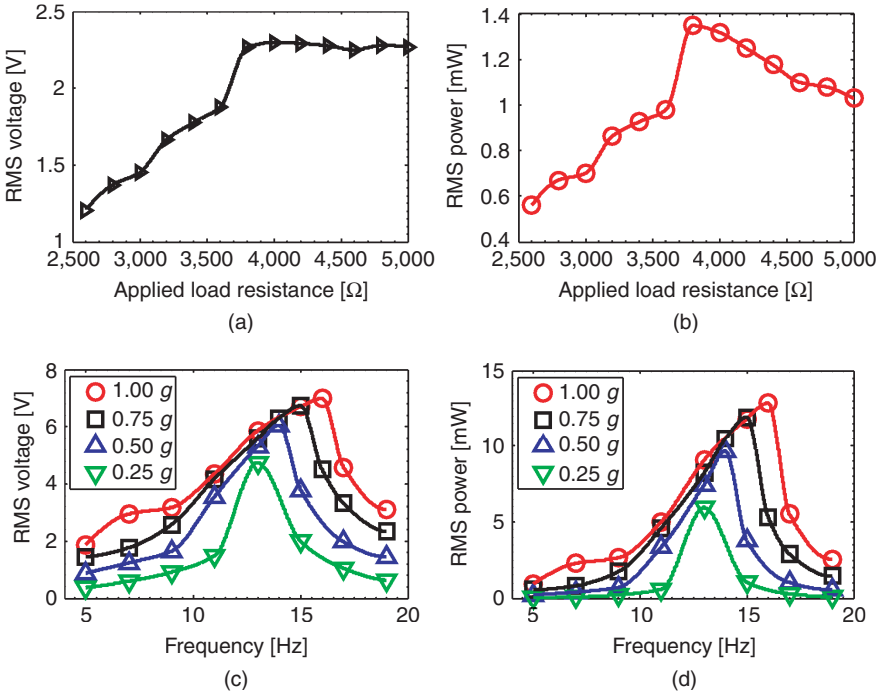

Figure 5 Experimental results. (a) RMS voltage as a function of the applied load resistance at 11 Hz (off resonance) and 0.25*g*, (b) RMS power as a function of the applied load resistance at 11 Hz (off resonance) and 0.25*g*, (c) RMS voltage response of the LIVE harvester across different base excitations as a function of frequency (at peak load of 3,800 Ω), and (d) RMS power response of the LIVE harvester across different base excitations as a function of frequency (at peak load of 3,800 Ω)

Table 3 Comparison of power densities in electromagnetic harvesters

Researcher	Frequency (Hz)	Base excitation (g)	Power (mW)	Normalized power density (mW cm^{-3} g^{-2})
Cepnik et al. (2011)	50	1	20.6	1.01
Byung-Chul et al. (2012)	16	0.2	1.52	1.07
Hatipoglu and Urey (2009)	24.4	15	0.4	0.017
Ching et al. (2002)	110	9.74	0.83	0.0087
Shuo and David (2010)	9.2	0.8	0.55	0.023
Saha et al. (2008)	2.75	1	2.46	0.194
Beeby et al. (2007)	52	0.06	0.005	4.5×10^{-8}
Marin et al. (2013)	50	0.2	25.5	0.541
Marin et al. (2012)	168	0.7	19	0.347
von Büren and Tröster (2007)	20	–	0.025	0.0096
Wang et al. (2012)	280	0.82	0.00212	0.101
Pan et al. (2006)	60	–	0.1	0.86
This work	13	0.25	5.9	15.33
This work	16	1	12.9	2.09

Charging a cellphone

To provide insight into the capability of the harvester for energy harvesting from human motion (such as running, walking, and hand movements), the harvester was shaken by hand to generate the voltage. The harvester was first tested by connecting it to the SigLab setup (Figure 6a), and the voltage response was recorded as shown in Figure 6b. The raw alternating voltage from the harvester had maximum amplitude of 14 V, and the

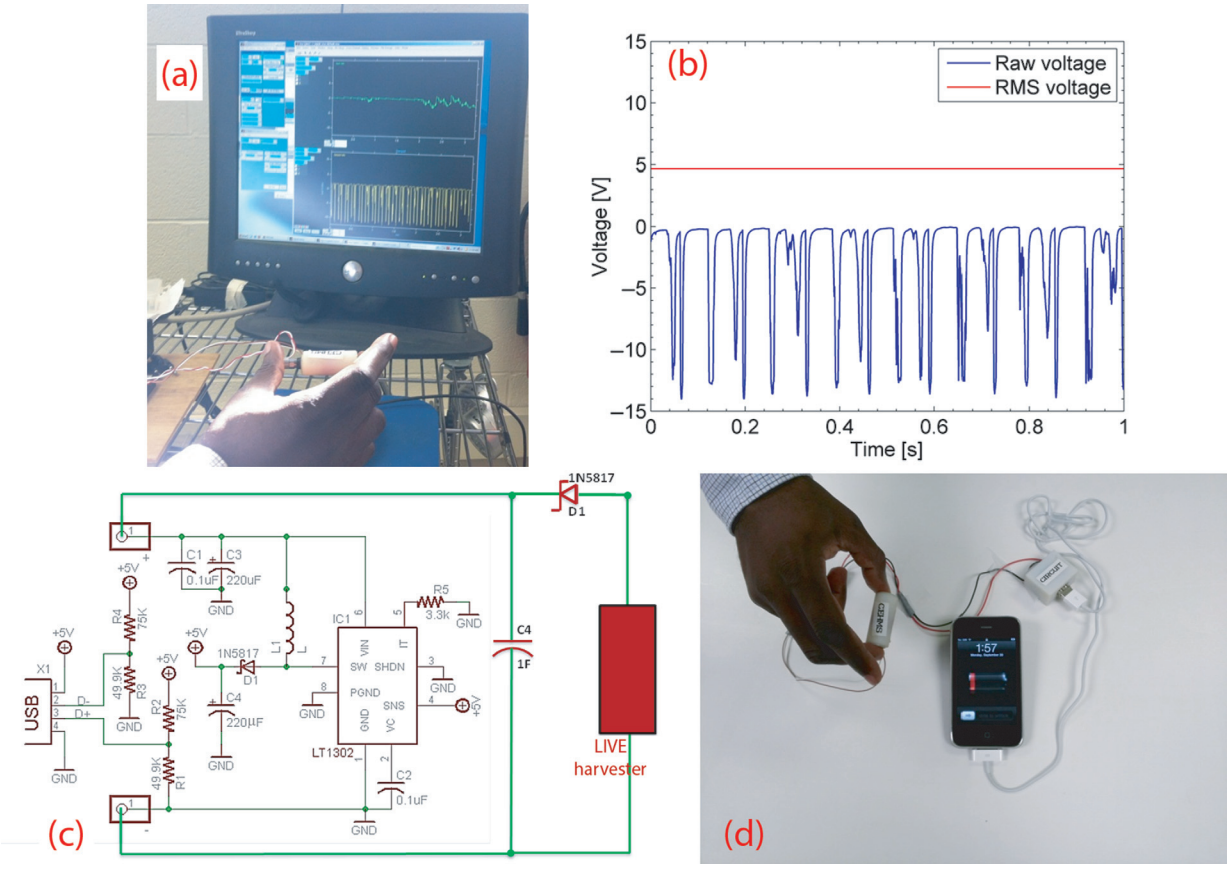

Figure 6 Harvester demonstration. (a) Hand-controlled harvester in voltage testing setup, (b) voltage response from the harvester being shaken by hand at a frequency of 7.44 Hz, (c) external charging circuit for the harvester, and (d) harvester being used to charge a cellphone

overall waveform corresponded to a frequency of approximately 7.44 Hz and RMS voltage of 4.7 V. The exhibited frequency (when compared with Figure 5c) occurred slightly above 1*g* acceleration and was slightly higher than observed in a human sprinter's motion (approximately 4–5 Hz). Figure 6c shows the external charging circuit designed for the harvester. It was built and used to supply constant 5 V DC and 500 mA to charge a cellphone via hand motion as shown in Figure 6d. The circuit was designed to convert AC to DC voltage and supply the DC voltage to the cellphone when it is within the range of $5\ \text{V} \pm 0.4\ \text{V}$.

Conclusions

An AA battery-sized harvester was modeled, fabricated, and tested. The harvester employed a double-repulsion configuration in the moving magnet composite which allowed for easy coil/magnet optimization. The double-repulsion configuration exhibited the lowest frequency, the highest displacement amplitude, and the largest velocity when compared to the no-repulsion and single-repulsion configurations. Furthermore, the double-repulsion configuration exhibited two strong regions of high magnetic flux which enabled efficient coil placement and significant voltage output. The double-repulsion LIVE harvester was found to exhibit RMS power output values of 5.9 mW at 0.25*g* and 12.9 mW at 1*g*. The harvester was also used to power a cellphone by supplying constant 4.7 V when shaken by hand.

Acknowledgment: The authors acknowledge the financial support from the National Science Foundation (NSF) through the INAMM program (S.P.) and through the ARMDEC (D.J.A.).

References

Aktakka, E. E., R. L. Peterson, and K. Najafi. 2011. "Thinned-PZT on SOI Process and Design Optimization for Piezoelectric Inertial Energy Harvesting." Paper presented at the 2011 16th International Conference on Solid-State Sensors, Actuators and Microsystems Conference (TRANSDUCERS), June 5–9.

Apo, D. J., M. Sanghadasa, and S. Priya. 2013. "*Low Frequency Arc-Based MEMS Structures for Vibration Energy Harvesting*." Paper presented at the 2013 8th IEEE International Conference on Nano/Micro Engineered and Molecular Systems (NEMS), April 7–10.

Apo, D. J., M. Sanghadasa, and S. Priya. 2014. "Vibration Modeling of Arc-Based Cantilevers for Energy Harvesting Applications." *Energy Harvesting and Systems* 1(1):1–12.

Beeby, S. P., R. N. Torah, M. J. Tudor, P. Glynne-Jones, T. O. Donnell, C. R. Saha, and S. Roy. 2007. "A Micro Electromagnetic Generator for Vibration Energy Harvesting." *Journal of Micromechanics and Microengineering* 17(7):1257.

Byung-Chul, L., R. Md Ataur, H. Seung-Ho, and C. Gwiy-Sang. 2012. "Low Frequency Driven Electromagnetic Energy Harvester for Self-Powered System." *Smart Materials and Structures* 21 (12):125024.

Cepnik, C., O. Radler, S. Rosenbaum, T. Ströhla, and U. Wallrabe. 2011. "Effective Optimization of Electromagnetic Energy Harvesters through Direct Computation of the Electromagnetic Coupling." *Sensors and Actuators A: Physical* 167(2):416–21. doi: http://dx.doi.org/10.1016/j.sna.2011.01.023.

Ching, N. N. H., H. Y. Wong, W. J. Li, P. H. W. Leong, and Z. Wen. 2002. "A Laser-Micromachined Multi-Modal Resonating Power Transducer for Wireless Sensing Systems." *Sensors and Actuators A: Physical* 97–98:685–90. doi: http://dx.doi.org/10.1016/S0924-4247(02)00033-X.

Dallago, E., M. Marchesi, and G. Venchi. 2010. "Analytical Model of a Vibrating Electromagnetic Harvester Considering Nonlinear Effects." *Power Electronics, IEEE Transactions on* 25 (8):1989–97. doi: 10.1109/tpel.2010.2044893.

Hatipoglu, G., and H. Urey. 2009. "FR4-Based Electromagnetic Energy Harvester for Wireless Tyre Sensor Nodes." *Procedia Chemistry* 1(1):1211–14. doi: http://dx.doi.org/10.1016/j.proche.2009.07.302.

Mann, B. P., and N. D. Sims. 2009. "Energy Harvesting From the Nonlinear Oscillations of Magnetic Levitation." *Journal of Sound and Vibration* 319(1–2):515–30. doi: http://dx.doi.org/10.1016/j.jsv.2008.06.011.

Marin, A., S. Bressers, and S. Priya. 2011. "Multiple Cell Configuration Electromagnetic Vibration Energy Harvester." *Journal of Physics D: Applied Physics* 44(29):295501.

Marin, A., P. Heitzmann, J. Twiefel, and S. Priya. 2012. "Improved Pen Harvester for Powering a Pulse Rate Sensor." Proc SPIE8341, Active and Passive Smart Structures and Integrated Systems 2012, 83411D, San Diego, CA, April 26. doi:10.1117/12.917013

Marin, A., J. Turner, D. S. Ha, and S. Priya. 2013. "Broadband Electromagnetic Vibration Energy Harvesting System for Powering Wireless Sensor Nodes." *Smart Materials and Structures* 22(7):075008.

Pan, C. T., Y. M. Hwang, H. L. Hu, and H. C. Liu. 2006. "Fabrication and Analysis of a Magnetic Self-Power Microgenerator." *Journal of Magnetism and Magnetic Materials* 304(1):e394–96. doi: http://dx.doi.org/10.1016/j.jmmm.2006.01.202.

Qi, Y., T. D. Nguyen, P. K. Purohit, and M. C. McAlpine. 2012. "Stretchable Piezoelectric Nanoribbons for Biocompatible Energy Harvesting." In *Stretchable Electronics*, edited by Takao Someya, 111–39. Weinheim, Germany: Wiley-VCH Verlag GmbH & Co. KGaA.

Saha, C. R., T. O'Donnell, N. Wang, and P. McCloskey. 2008. "Electromagnetic Generator for Harvesting Energy from Human Motion." *Sensors and Actuators A: Physical* 147(1):248–53. doi: http://dx.doi.org/10.1016/j.sna.2008.03.008.

Shuo, C., and P. A. David. 2010. "A Study of a Multi-Pole Magnetic Generator for Low-Frequency Vibrational Energy Harvesting." *Journal of Micromechanics and Microengineering* 20(2):025015.

Singh, S. P., K. Saha, J. Singh, and A. P. S. Sandhu. 2012. "Measurement and Analysis of Vibration and Temperature Levels in Global Intermodal Container Shipments on Truck, Rail and Ship." *Packaging Technology and Science* 25(3):149–60. doi: 10.1002/pts.968.

Tornincasa, S., M. Repetto, E. Bonisoli, and F. Di Monaco. 2012. "Optimization of Magneto-Mechanical Energy Scavenger for Automotive Tire." *Journal of Intelligent Material Systems and Structures* 23(18):2055–64. doi: 10.1177/1045389x11430741.

von Büren, T., and G. Tröster. 2007. "Design and Optimization of a Linear Vibration-Driven Electromagnetic Micro-Power Generator." *Sensors and Actuators A: Physical* 135(2):765–75. doi:http://dx.doi.org/10.1016/j.sna.2006.08.009.

Wang, P., H. Liu, X. Dai, Z. Yang, Z. Wang, and X. Zhao. 2012. "Design, Simulation, Fabrication and Characterization of a Micro Electromagnetic Vibration Energy Harvester with Sandwiched Structure and Air Channel." *Microelectronics Journal* 43(2):154–59. doi: http://dx.doi.org/10.1016/j.mejo.2011.10.003.

Zavodney, L. D., and A. H. Nayfeh. 1989. "The Non-Linear Response of a Slender Beam Carrying a Lumped Mass to a Principal Parametric Excitation: Theory and Experiment." *International Journal of Non-Linear Mechanics* 24(2):105–25. doi: http://dx.doi.org/10.1016/0020-7462(89)90003-6.

Zhou, Y., D. J. Apo, and S. Priya. 2013. "Dual-Phase Self-Biased Magnetoelectric Energy Harvester." *Applied Physics Letters* 103 (19). doi: http://dx.doi.org/10.1063/1.4829151.